Controlled Growth of Two-Dimensional and One-Dimensional ZnO Nanostructures on Indium Tin Oxide Coated Glass by Direct Electrodeposition

Debabrata Pradhan and Kam Tong Leung*

WATLab and Department of Chemistry, University of Waterloo, Waterloo, Ontario N2L 3G1, Canada

Received March 21, 2008. Revised Manuscript Received June 6, 2008

A simple electrochemical deposition technique is used to deposit ZnO nanostructures with diverse morphology directly on ITO-coated glass substrates at 70 °C. The concentration of the $Zn(NO_3)_2 \cdot 6H_2O$ electrolyte is important to controlling the dimensionality of the nanostructures, with formation of one-dimensional (1D) nanospikes and nanopillars (with 50−500 nm diameter) below 0.01 M and of two-dimensional (2D) nanowalls and nanodisks (with 50−100 nm wall/disk thickness) above 0.05 M. Glancing-incidence X-ray diffraction study shows their wurtzite structure and confirms the change in the preferred crystal plane orientation with the dimensionality of ZnO nanostructures. UV−vis spectroscopy reveals a higher transmittance from 2D nanostructures than from 1D nanostructures and their optical direct band gaps estimated to be 3.12−3.27 eV. Depth-profiling X-ray photoemission studies show the presence of $Zn(OH)_2$ outer layers on the ZnO nanostructures, with a higher $Zn(OH)_2$ moiety for 2D nanostructures relative to 1D nanostructures. Furthermore, a substantial quantity of Cl (provided by the KCl supporting electrolyte) is detected throughout the 2D nanostructures only. The photoemission data therefore affirm our proposed growth mechanism that involves capping of the preferred [0001] growth direction by Cl^- ions under fast hydroxylation kinetics condition as observed at a higher $Zn(NO_3)_2 \cdot 6H_2O$ electrolyte concentration.

1. Introduction

Oriented nanostructures are extremely desirable in many applications, but fabricating such complex structures remains challenging. Zinc oxide (ZnO) is one of the few marvelous semiconducting and piezoelectric materials that form self-assembled nanostructures of specific orientation, offering numerous opportunities for applications in nanogenerators,[1] rectifying diodes,[2] pH meters,[3] sensors,[4] and electron emitters.[5] The feasibility of ZnO for these applications is due to the successful synthesis of diverse ZnO nanostructures,[6] including nanorings, nanobows, nanohelixes, nanosprings, nanobelts, nanotubes, nanopropellers, nanodisks, and nanocombs, by thermal evaporation or chemical vapor deposition (CVD) method. The formation of these unique and novel ZnO nanostructures is ascribable to its three fastest growth directions: [0001], [01$\bar{1}$0], and [2$\bar{1}\bar{1}$0], and to the ±(0001) polar surfaces.[6] In the CVD process, the use of high temperature for growing ZnO nanomaterials is necessary due to the high melting point (1975 °C) of the source materials.[7] High growth temperature, however, limits the types of substrates and the scope of the phase space in which new nanostructures could be deposited. It would therefore be of great interest to develop alternative techniques to synthesize these materials at lower temperatures. In such regard, electrochemical and wet-chemistry (hydrothermal or solvothermal) methods are the most appealing.[8−10] Furthermore, unlike the wet-chemistry method, in which the substrate has to be dipped inside the requisite solution often for days to form ZnO nanostructures,[11,12] electrochemical deposition requires only 1 min to 2 h to grow such nanostructures at relatively lower temperature (<90 °C),[8] making it one of the best low-temperature growth methods available for conducting substrates to date.

The major advantages in using the electrochemical deposition technique to grow ZnO nanostructured materials are (1) catalyst-free growth, (2) low growth temperature, and (3) inexpensive substrate (indium tin oxide-coated glass or ITO-glass). The catalyst-free growth of ZnO offers excellent opportunities to be used in many electronic and optical applications, while the growth of ZnO near ambient temperature opens up the prospect of deposition on plastic substrates. In a recent study, Gao et al. also reported the growth of ZnO nanowires on a plastic substrate using a hydrothermal technique.[13] In the CVD growth process, expensive sapphire substrates (that can withstand the high deposition temperature) have been used to grow the ZnO nanostructures.[6] Recently, ZnO nanowires and nanobelts have also been grown on ZnO films or bulk ZnO substrate by thermal evaporation of zinc powder.[14,15] The choice of these substrate materials is governed by the requirement for lattice matching and preferential growth along the *c*-axis direction. The biggest advantage of the electrodeposition and hydrothermal techniques has therefore been demonstrated in the successful growth of ZnO nanomaterials on

* Corresponding author, tong@uwaterloo.ca.

(1) Wang, Z. L.; Song, J. *Science* **2006**, *312*, 242.
(2) Lao, C. S.; Liu, J; Gao, P; Zhang, L.; Davidovic, D.; Rao, T.; Wang, Z. L. *Nano Lett.* **2006**, *6*, 263.
(3) Kang, B. S.; Ren, F.; Heo, Y. W.; Tien, L. C.; Norton, D. P.; Pearton, S. J. *Appl. Phys. Lett.* **2005**, *86*, 112105.
(4) Rout, C. S.; Krishna, S. H.; Vivekchand, S. R. C.; Govindaraj, A.; Rao, C. N. R. *Chem. Phys. Lett.* **2006**, *418*, 586.
(5) Wei, A.; Sun, X. W.; Xu, C. X.; Dong, Z. L.; Yu, M. B.; Huang, W. *Appl. Phys. Lett.* **2006**, *88*, 213102.
(6) Gao, P. X.; Lao, C. S.; Ding, Y.; Wang, Z. L. *Adv. Funct. Mater.* **2006**, *16*, 53, and references therein.
(7) Kong, X. Y.; Ding, Y.; Yang, R.; Wang, Z. L. *Science* **2004**, *303*, 1348.
(8) Peulon, S.; Lincot, D. *Adv. Mater.* **1996**, *8*, 166.
(9) Vayssieres, L. *Adv. Mater.* **2003**, *15*, 464.
(10) Kar, S.; Dev, A.; Chaudhuri, S. *J. Phys. Chem. B* **2006**, *110*, 17848.
(11) Tian, Z. R.; Voigt, J. A.; Liu, J.; Mckenzie, B.; Mcdermott, M. J.; Rodriguez, M. A.; Konishi, H.; Xu, H. *Nat. Mater.* **2003**, *2*, 821.
(12) Yamabi, S.; Imai, H. *J. Mater. Chem.* **2002**, *12*, 3773.
(13) Gao, P. X.; Song, J.; Liu, J.; Wang, Z. L. *Adv. Mater.* **2007**, *19*, 67.
(14) Pradhan, A. K.; Williams, T. M.; Zhang, K.; Hunter, D.; Dadson, J. B.; Lord, K.; Roy, U. N.; Cui, Y.; Burge, A. *J. Nanosci. Nanotechnol.* **2006**, *6*, 1985.
(15) Wen, X.; Fang, Y.; Pang, Q.; Yang, C.; Wang, J.; Ge, W.; Wong, K. S.; Yang, S. *J. Phys. Chem. B* **2005**, *109*, 15303.

10.1021/la8008943 CCC: $40.75
Published on Web 07/24/2008

inexpensive glass (and plastic) substrates itself.[8,11,13,16] Furthermore, ZnO is believed to exhibit one of the best electron emission characteristics among wide band gap semiconducting materials.[5] Deposition of ZnO nanostructures (especially nanopillars and nanospikes) on ITO substrates therefore has potential applications in display technology. Another striking advantage of the electrodeposition technique over thermal transport method is the consumption of lesser quantity of source material per unit substrate area for ZnO nanostructures growth. In the thermal transport method, normally >1 g of ZnO powder is required for deposition over a 1 cm^2 substrate area at high temperature.[17,18] In contrast, <100 mg of zinc salt is needed to grow nanostructured materials on the same substrate size in electrochemical technique. Moreover, the same electrolyte solution can be reused for several runs, further improving the economy of producing the ZnO nanomaterials. Hydrothermal synthesis is also a competent method for producing a large quantity of ZnO nanomaterials, but it often employs relatively harsh chemicals such as methylamine or other amine complex,[13,16] in contrast to electrodeposition in which simple aqueous salt solutions are normally used.

Earlier studies on electrochemical deposition of ZnO have been mostly devoted to growth of thin films.[19−22] After the pioneering work on electrodeposition of ZnO nanorods and thin films by Peulon et al.[8] and Izaki et al.,[19,23] there have since been a number of more recent studies on the electrochemical synthesis of one-dimensional (1D) ZnO nanorods on various substrates, including GaN,[24,25] ITO,[26,27] SnO_2,[8,28,29] Au/Si,[30,31] ZnO films,[32] and Zn foils.[33,34] However, there is only a rather limited amount of work on the two-dimensional (2D) ZnO nanostructures, most of which report nanoplatelet-like deposits not vertically grown on the substrate.[32,35−38] In the present work, we demonstrate the formation of diverse, well-defined ZnO nanostructures, including nanowalls, nanodisks, nanospikes, and nanopillars, on ITO-glass substrates in a template-free electrodeposition process. Both nanowalls and nanopillars are found to be well-aligned and perpendicular to the ITO-glass substrate. In addition, extensive X-ray photoelectron spectroscopy (XPS) studies have been performed for the first time to determine the effect of electrolytic components on the growth mechanism of these intriguing 2D (nanowalls and nanodisks) and 1D ZnO nanostructures (nanospikes and nanopillars).

2. Experimental Details

The electrochemical deposition experiments were carried out in a three-electrode glass cell immersed in a water bath held at 70 °C. The working electrode was single-sided polished, SiO_2-passivated float glass coated with an ITO film (200−500 nm thick with a sheet resistance of 4−8 Ω) obtained from Delta Technologies Limited (Minnesota, USA). The ITO surface was found to be extremely smooth with a root mean square roughness of 0.4 nm as measured by atomic force microscopy (Digital Instruments Nanoscope IV). A Ag/AgCl electrode was used as the reference electrode while a platinum wire served as the counter electrode. An aqueous solution (15 mL) of $Zn(NO_3)_2 \cdot 6H_2O$ (Aldrich) of varying molar concentrations (used as the electrolyte) was mixed with 0.1 M KCl (used as the supporting electrolyte) for the electrodeposition. The exposed area of working electrode was either 10 × 5 or 15 × 15 mm^2. A potentio/galvanostat electrochemical workstation (CH Instruments 660A) was used to deposit the nanostructures by amperometry potentiostatically at −1.1 V (relative to the Ag/AgCl reference electrode). The deposition times used to grow the 2D (nanowalls and nanodisks) and 1D nanostructures (nanospikes and nanopillars) were 1 and 2 h, respectively. After deposition, the resulting nanodeposits were thoroughly rinsed with Millipore water and dried under a nitrogen gas stream. The morphologies of the resulting nanodeposits were analyzed by using a LEO FESEM 1530 field-emission scanning electron microscope (SEM), equipped with an EDAX Pegasus 1200 energy-dispersive X-ray analysis system (EDX). The crystal structure of the nanodeposits was characterized by glancing-incidence X-ray diffraction (GIXRD) using a PANalytical X'Pert Pro MRD diffractometer with Cu Kα radiation (1.54 Å) and an incidence angle omega = 0.3°. The optical properties of the ZnO nanostructures were measured with a Perkin-Elmer Lambda 35 UV−vis spectrometer equipped with a Labsphere integrating sphere. The surface composition of the ZnO nanostructures was analyzed by XPS using a Thermo-VG Scientific ESCALab 250 Microprobe with a monochromatic Al Kα source (1486.6 eV), capable of an energy resolution of 0.4−0.5 eV full width at half-maximum (fwhm).

3. Results and Discussion

3.1. Morphology. Figure 1 shows the scanning electron microscopy (SEM) images of four different ZnO nanostructures electrochemically grown on ITO-coated glass substrates. The observed structural variation can be achieved by simply changing the zinc nitrate electrolyte concentration, with the concentration of the KCl supporting electrolyte fixed at 0.1 M. At 0.1 M $Zn(NO_3)_2 \cdot 6H_2O$ (with 0.1 M KCl), 2D wall-like structures with thickness of 50−100 nm were vertically grown on the substrate (Figure 1a,b). The length of these nanowalls varies from hundreds of nanometers to several micrometers. Previously Xu et al. obtained nanoplatelets with a large thickness range of 70−400 nm,[37] and very recently Cao et al. produced ZnO nanosheets on a Zn-seeded layer by controlling the electrochemical currents.[32] These 2D ZnO nanostructures were found to be randomly distributed and generally self-terminated in the lateral direction, which may be due to the lower electrolyte concentration (0.05 M) used in the electrodeposition.[32,37] In contrast, the well-defined nanowalls obtained in the present work (Figure 1a) appear to be denser and to grow perpendicular to the ITO substrate. Growth in the lateral direction evidently ceases when one nanowall meets

(16) Greene, L. E.; Law, M.; Goldberger, J.; Kim, F.; Johnson, J. C.; Zhang, Y.; Saykally, R. J.; Yang, P. *Angew. Chem., Int. Ed.* **2003**, *42*, 3031.
(17) Gao, P. X.; Ding, Y.; Mai, W.; Hughes, W. L.; Lao, C.; Wang, Z. L. *Science* **2005**, *309*, 1700.
(18) Xing, Y. J.; Xi, Z. H.; Xue, Z. Q.; Zhang, X. D.; Song, J. H.; Wang, R. M.; Xu, J.; Song, Y.; Zhang, S. L.; Yu, D. P. *Appl. Phys. Lett.* **2003**, *83*, 1689.
(19) Izaki, M.; Omi, T. *J. Electrochem. Soc.* **1996**, *143*, L53.
(20) Pauporte, T.; Lincot, D. *J. Electrochem. Soc.* **2001**, *148*, C310.
(21) Choi, K.; Lichtenegger, H. C.; Stucky, G. D.; McFarland, E. W. *J. Am. Chem. Soc.* **2002**, *124*, 12402.
(22) Li, M.; Zhai, J.; Liu, H.; Song, Y.; Jiang, L.; Zhu, D. *J. Phys. Chem. B* **2003**, *107*, 9954.
(23) Izaki, M.; Omi, T. *Appl. Phys. Lett.* **1996**, *68*, 2439.
(24) Pauporte, T.; Lincot, D.; Viana, B.; Pelle, F. *Appl. Phys. Lett.* **2006**, *89*, 233112.
(25) Pauporte, T.; Cortes, R.; Froment, M.; Beaumont, B.; Lincot, D. *Chem. Mater.* **2002**, *14*, 4702.
(26) Chen, Q. P.; Xue, M. Z.; Sheng, Q. R.; Liu, Y. G.; Ma, Z. F. *Electrochem. Solid-State Lett.* **2006**, *9*, C58.
(27) Anthony, S. P.; Lee, J. I.; Kim, K. J. *Appl. Phys. Lett.* **2007**, *90*, 103107.
(28) Levy-Clement, C.; Tena-Zaera, R.; Ryan, M. A.; Katty, A.; Hodes, G. *Adv. Mater.* **2005**, *17*, 1512.
(29) Tena-Zaera, R.; Elias, J.; Wang, G.; Levy-Clement, C. *J. Phys. Chem. C* **2007**, *111*, 16706.
(30) Cao, B.; Li, Y.; Duan, G.; Cai, W. *Cryst. Growth Des.* **2006**, *6*, 1091.
(31) Izaki, M.; Shinagawa, T.; Takahashi, H. *J. Phys. D: Appl. Phys.* **2006**, *39*, 1481.
(32) Cao, B.; Teng, X.; Heo, S. H.; Li, Y.; Cho, S. O.; Li, G.; Cai, W. *J. Phys. Chem. C* **2007**, *111*, 2470.
(33) Yang, J.; Liu, G.; Lu, J.; Qiu, Y.; Yang, S. *Appl. Phys. Lett.* **2007**, *90*, 103109.
(34) Wong, M. H.; Berenov, A.; Qi, X.; Kappers, M. J.; Barber, Z. H.; Illy, B.; Lockman, Z.; Ryan, M. P.; MacManus-Driscoll, J. L. *Nanotechnology* **2003**, *14*, 968.
(35) Yoshida, T.; Tochimoto, M.; Schlettwein, D.; Woehrle, D.; Sugiura, T.; Minoura, H. *Chem. Mater.* **1999**, *11*, 2657.
(36) Illy, B.; Shollock, B. A.; MacManus-Driscoll, J. L.; Ryan, M. P. *Nanotechnology* **2005**, *16*, 320.
(37) Xu, L.; Guo, Y.; Liao, Q.; Zhang, J.; Xu, D. *J. Phys. Chem. B* **2005**, *109*, 13519.
(38) Gao, Y.; Nagai, M. *Langmuir* **2006**, *22*, 3936.

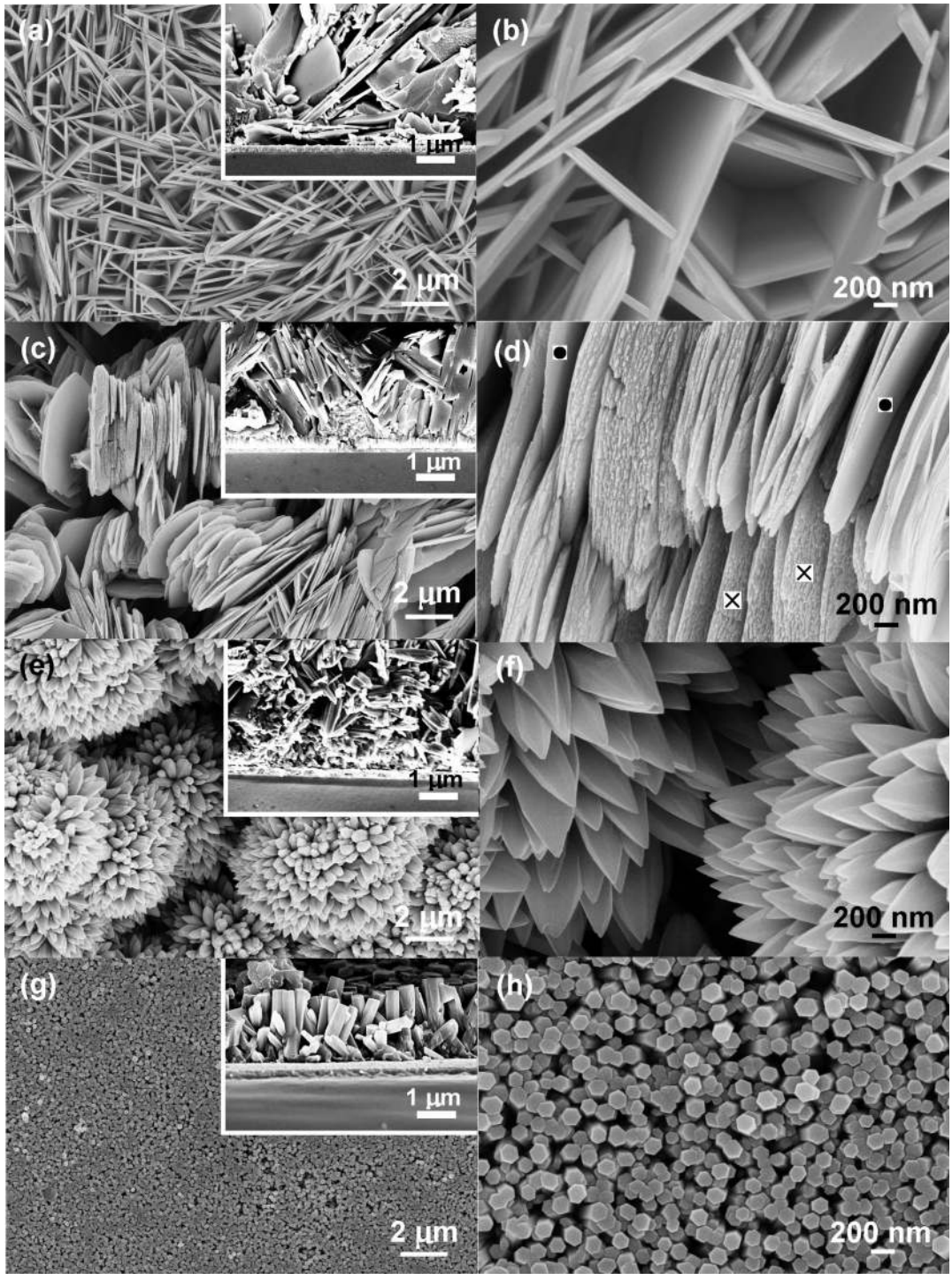

Figure 1. SEM images of (a, b) ZnO nanowalls, (c, d) nanodisks, (e, f) nanospikes, and (g, h) nanopillars grown on ITO-glass at 70 °C with 0.1 M KCl solution and varying $Zn(NO_3)_2 \cdot 6H_2O$ concentrations of 0.1, 0.05, 0.01, and 0.001 M, respectively. Insets show the corresponding cross sectional images.

another (at 60−90°), often making compartments with well-defined nooks (Figure 1b). The apparent extended growth of the nanowalls, terminated only by intercepting walls, is likely due to faster hydroxylation reaction kinetics at a high $Zn(NO_3)_2 \cdot 6H_2O$ electrolyte concentration (0.1 M) used for electrodeposition in the present work. Additionally, a large fraction of the nanowalls tends to form local groups in nearly parallel arrangement (Figure 1a). These vertical nanowalls with a gap of 100−800 nm offer a higher surface area appropriate for solar cell applications. We also observe that the thickness of these ZnO nanowalls can be controlled by changing the electrolyte concentration, and wall thickness as large as $\sim 1\,\mu$m can be obtained at 0.5 M. Deposition of nanowalls has also been carried out at 70 °C as a function of deposition time in order to understand the growth evolution. In particular, in the early growth stage with a deposition time of 1 s, ZnO forms as spherical nanoparticles, with a few taking on an elongated shape and appearing as nanobars. At a longer deposition time of 30−60 s, ZnO appears as nanoplatelets, and they eventually become distinct nanowalls at a deposition time of 300 s. Upon further increasing the deposition time to 1 h, we observe no discernible change in the morphology except an increase in the thickness of the film. The wall thickness of the

nanowalls (i.e., the ledge width) appears to remain nearly constant with the deposition time. The corresponding cross-sectional SEM image (inset of Figure 1a) shows the absence of a ZnO buffer layer prior to the onset of nanowalls growth. The overall thickness of the nanowalls film was measured to be ~50 μm for a 1 h deposition on a 10 × 5 mm^2 area in 15 mL of electrolyte solution. It should be noted that Izaki et al. reported that the growth rate of the ZnO film is the highest at an electrolyte concentration of 0.1 M.[19]

At a reduced electrolyte concentration of 0.05 M $Zn(NO_3)_2 \cdot 6H_2O$ (with 0.1 M KCl), electrodeposition produced a large quantity of stacked ZnO nanodisks, 3−5 μm in diameter and ~50 nm thick (Figure 1c,d). The SEM image obtained at a higher magnification reveals that one side of the disks is smoother than the other. The smooth and rough surfaces of nanodisks are marked by the symbols • and ×, respectively, in Figure 1d. Some of the stacked nanodisks are found to be randomly oriented. With the exception of the stacking, the morphology and random orientation of the nanodisks are similar to the nanoplatelets reported earlier.[32,37] It should be noted that Yoshida et al. also reported stacking of nanodisks, circular in shape, obtained by electrodeposition in an aqueous solution of zinc nitrate mixed with water-soluble tetrasulfonated metallophthalocyanines.[35] In the present work, most of the nanodisks appear to be hexagonal in shape, with some hexagons exhibiting rounded vertices. The differences in the shape of the nanodisks may be due to the nature of the supporting electrolytes. The corresponding cross sectional image (inset of Figure 1c) shows no ZnO buffer layer and the appearance of nanowall-type structures directly on the ITO substrate. The film thickness is measured to be almost half (24.0 μm) of that of the nanowall film obtained with the same deposition time (1 h).

Electrodeposition carried out at 0.01 M $Zn(NO_3)_2 \cdot 6H_2O$ (with 0.1 M KCl) gave rise to the formation of nanospikes arranged in globular bunches (6−8 μm diameter) that are remarkably similar to Cadamba flower (botanical name *Anthocephalus cadamba*) as shown in Figure 1e,f. The nanospikes in individual globular bunches are found to have hexagonal trunk (200−500 nm diameter) with a sharp tapering tip (20−50 nm diameter). The corresponding magnified SEM image shows that the nanospikes in each globular bunch are held together by very fine threads of diameter less than 10 nm (not shown). However, in the region where these nanospikes do not form globes, the nanospikes appear to be devoid of any interconnecting threads. The corresponding cross sectional image (inset of Figure 1e) shows random growth of nanospikes with no preferred alignment. The corresponding film thickness is found to be 12 μm for a deposition time of 2 h on a 10 × 5 mm^2 substrate area in a 15 mL electrolyte solution.

Further decreasing the $Zn(NO_3)_2 \cdot 6H_2O$ electrolyte concentration to 0.001 M (with 0.1 M KCl) in the electrodeposition produced well-aligned nanopillars on the ITO-glass substrate. Figure 1g,h shows the SEM images of high-density (5 × 10^9 cm^{-2}), vertically aligned ZnO nanopillars with well-defined hexagonal flat tops with some of them appearing to merge with one another. The typical dimensions of individual nanopillars are 100−120 nm in diameter and ~2 μm long. The length has been estimated from the corresponding cross-sectional SEM image (inset of Figure 1g), which also shows the absence of ZnO buffer layer prior to the formation of nanopillars. In a recent study, Chen et al. obtained nanopillars of larger diameters (100−250 nm) at a lower density on ITO-glass using the same electrolyte, with the majority of nanopillars not being vertically aligned.[26] However, higher degrees of orientation and alignment of ZnO nanorods have been observed on GaN single crystal by Pauporte et al.[24] and on ZnO-seeded layers by Cao et al.,[32] which might be due to their close lattice parameters. This is contrary to the work by Liu et al. that demonstrates that lattice matching is not a primary requirement in the electrodeposition of ZnO nanopillars on single-crystal gold.[39] The present work therefore shows that well-aligned ZnO nanopillars can be grown vertically on virgin ITO-glass (i.e., without a seed layer) by using an appropriate potential and optimum electrolyte concentration. The length and, to a certain extent, the density of these pillars can also be varied by controlling the deposition time. Nanopillars with diameter less than 50 nm can also be obtained at a lower electrolyte concentration (0.0005 M). It should be noted that the flat top surfaces of ZnO nanopillars produced in the present catalyst-free method are of great interest in the lasing applications.[40] These high-density, self-assembled nanopillars on ITO-glass substrate can also potentially be used as new materials for flat panel displays and photonic and electronic devices.[1] Furthermore, the nanopillars can be harvested and used for nanoscale field effect transistors and biological sensors and in new device applications.[1–5]

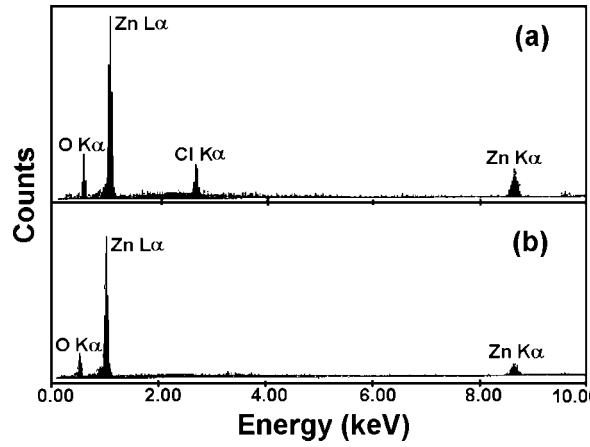

Figure 2. EDX spectra of (a) ZnO nanowalls and (b) nanopillars grown on ITO-glass at 70 °C.

Table 1. Elemental Compositions (in atom %) for Zn, O, and Cl Obtained by EDX Analysis and the Corresponding Zn-to-O Atomic Ratios for ZnO Nanowalls, Nanodisks, Nanospikes, And Nanopillars

	atomic percent			
ZnO	Zn	O	Cl	Zn:O
nanowalls	43.0	48.9	8.1	0.90
nanodisks	47.5	45.2	7.3	1.05
nanospikes	55.0	43.8	1.2	1.28
nanopillars	52.7	45.1	0.6	1.16

Energy dispersive X-ray (EDX) analysis has been performed in order to determine the elemental composition of the as-deposited ZnO nanostructures. Figure 2 compares the representative EDX spectra of ZnO nanowalls and nanopillars. It should be noted that the EDX spectrum of nanowalls (Figure 2a) is similar to that of nanodisks (not shown), while the spectrum of nanopillars (Figure 2b) is similar to that of nanospikes (not shown). Table 1 compares the corresponding elemental compositions of different nanostructures electrodeposited on ITO-glass substrates. Evidently, none of the nanostructures gives the expected unity

(39) Liu, R.; Vertegel, A. A.; Bohannan, E. W.; Sorenson, T. A.; Switzer, J. A. *Chem. Mater.* **2001**, *13*, 508.
(40) Zou, B.; Liu, R.; Wang, F.; Pan, A.; Cao, L.; Wang, Z. L. *J. Phys. Chem. B* **2006**, *110*, 12865.

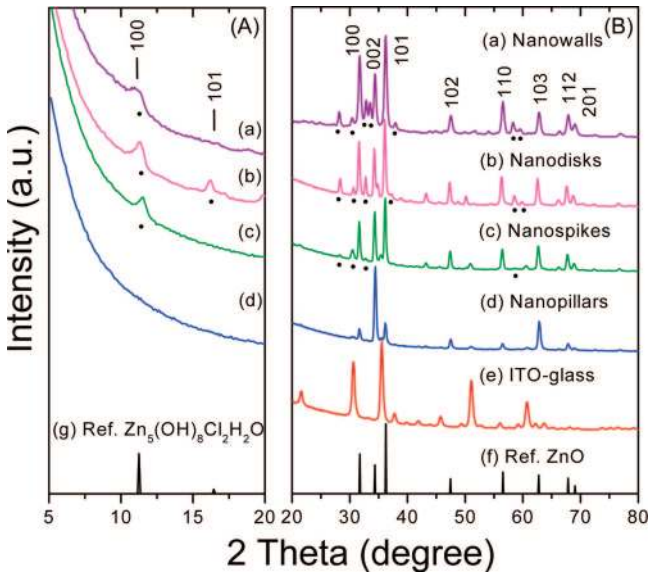

Figure 3. Glancing-incidence XRD spectra collected at (A) small 2θ and (B) over extended 2θ range for (a) ZnO nanowalls, (b) nanodisks, (c) nanospikes, and (d) nanopillars electrodeposited on ITO-glass at 70 °C. The crystallographic identifications of the ZnO peaks are labeled and compared with (e) the XRD spectrum of ITO-glass and (f) the bar chart of the reference ZnO powder (JCPDS 01-076-0704). The features marked by solid circles are assigned to (g) $Zn_5(OH)_8Cl_2 \cdot H_2O$ (JCPDS 00-007-0155).

Zn-to-O stoichiometric ratio. The smaller Zn-to-O ratios for nanowalls and nanodisks in comparison to nanospikes and nanopillars are possibly due to their higher $Zn(OH)_2$ mole percentage as observed from the XPS measurements discussed below. Moreover, the >1.0 stoichiometric ratios found for nanodisks, nanospikes, and nanopillars are in good agreement with the previous report on ZnO thin films (1.58)[41] and nanosheets (1.16).[42] Despite the use of KCl solution with the same concentration (0.1 M) for all the electrodeposition, it is interesting to observe a substantial quantity of Cl impurities (>7 atom %) in the 2D nanostructures (nanowalls and nanodisks) but negligible Cl content (<2 atom %) in the 1D nanostructures (nanospikes and nanopillars), which suggests that Cl may play an important role in the formation of these 2D ZnO nanostructures (see later). The presence of Cl may also indicate the presence of chlorinated salts in the 2D ZnO nanostructures formed during growth at a higher electrolyte concentration (>0.01 M).[43]

3.2. Structural Properties. Figure 3 shows the corresponding glancing incidence X-ray diffraction (GIXRD) patterns of ZnO nanowalls, nanodisks, nanospikes, and nanopillars electrodeposited on ITO-glass substrates. The positions of the more prominent diffraction peaks (Figure 3B, curves a−d) are in good accord with those of the wurtzite (hexagonal) ZnO structure (JCPDS 01-076-0704, Figure 3B, curve f). For nanowalls (Figure 3B, curve a) and nanodisks (Figure 3B, curve b), additional features with discernible intensities (marked by solid circles in Figure 3) are also observed. These weaker features appear to be in better match with the XRD reference pattern of the hydroxyl compound $Zn_5(OH)_8Cl_2 \cdot H_2O$ (or $ZnCl_2 \cdot 4Zn(OH)_2 \cdot H_2O$, JCPDS 00-007-0155), known to form at an electrolyte concentration >0.01 M,[43] than that of the leafy ZnO crystal (JCPDS 00-021-1486). To further ensure the correct identification, we extend our GIXRD scans to small 2θ angles in order to search for the primary peak of the hydroxyl compound. Evidently, the presence of the diffraction feature at ~11.2° (Figure 3A) therefore affirms the formation of the $Zn_5(OH)_8Cl_2 \cdot H_2O$ in nanowalls, nanodisks, and nanospikes. Peulon et al. also carried out a mechanistic study on the cathodic electrodeposition of ZnO films and related hydroxyl compounds, including $ZnO_x(OH)_y$ and $Zn(OH)_xCl_y$, in $ZnCl_2$ solutions.[43] They inferred that the formation of these hydroxyl compounds occurs when the ionic products of the corresponding ions are higher than the solubility product. This situation arises when the Zn^{2+} concentration is greater than 0.01 M (with 0.1 M KCl), which is in good agreement with the present results that shows the presence of $Zn_5(OH)_8Cl_2 \cdot H_2O$ XRD features in the nanostructures (nanowalls, nanodisks, and nanospikes) obtained at the higher $Zn(NO_3)_2 \cdot 6H_2O$ concentration of ≥0.01 M but not in nanopillars obtained at 0.001 M $Zn(NO_3)_2 \cdot 6H_2O$.

From the locations of the assigned ZnO diffraction features, the lattice parameters of all the ZnO nanostructures are calculated and listed in the Table 2. Evidently, the calculated values of $a = b = 3.24-3.26$ Å and $c = 5.20-5.23$ Å are in good accord with the corresponding literature values of $a = b = 3.2530$ Å and $c = 5.2130$ Å of the reference ZnO powder (JCPDS 01-076-0704). Moreover, the peak intensities of the ZnO features are found to vary with the morphology of the nanostructures. For ZnO nanowalls (Figure 3B, curve a) and nanodisks (Figure 3B, curve b), the (101) and (100) peaks appear to be more intense, indicating their preferred growth directions. The relative intensity of the (002) peak is found to increase for the ZnO nanospikes (Figure 3B, curve c) particularly with respect to the reference pattern, suggesting the beginning of the *c*-axis oriented growth. However, due to the random growth direction of the nanospikes, other peaks are also present. For ZnO nanopillars, the relative intensity of the (002) peak is found to be the singular most intense feature, with the (100) and (101) peak intensities drastically reduced (Figure 3B, curve d), which is as expected from their better aligned *c*-axis growth. The most intense (002) diffraction peak from the nanopillars also exhibits a fwhm of 0.35°, in excellent accord with that found for the CVD-grown ZnO nanowires at 760 °C.[14] This illustrates the high crystallinity of the ZnO nanopillars electrochemically grown at 70 °C in the present work. The other less intense peaks in Figure 3B, curve d, can be attributed to a small fraction of the nonaligned nanopillars. A more quantitative comparison of individual diffraction intensities among the ZnO nanostructures with respect to the reference (JCPDS 01-076-0704) can be made from the crystallographic orientation index $M(hkl)$, shown in Table 2. In particular, $M(002)$ and $M(103)$ are found to increase with decreasing electrolyte concentration that leads to structural evolution from nanowalls to nanopillars, while a generally opposite trend in $M(hkl)$ is found for all remaining crystal planes.

3.3. Optical Properties. The optical properties of ZnO nanostructures were examined by using UV−vis spectroscopy. Figure 4A shows the transmittance (T%) as a function of wavelength for the as-grown ZnO nanostructures shown in Figure 1, along with a reference spectrum from the ITO-glass substrate. As expected, all the as-deposited ZnO samples (Figure 4A, curves a−d) exhibit a lower transmittance compared to the bare ITO-glass (Figure 4A, curve e). An apparent reduction in T% is observed as the morphology evolves from nanowalls (2D) to nanopillars (1D). However, the T% for the nanowalls (77% at 600 nm) is found to be slightly higher than that of the electrochemically synthesized (smooth) ZnO films obtained at −1.0 V (72% at 600 nm).[23] The variation in T% of different ZnO

(41) Tan, S. T.; Sun, X. W.; Zhang, X. H.; Chua, S. J.; Chen, B. J.; Teo, C. C. *J. Appl. Phys.* **2006**, *100*, 033502.
(42) Hu, J. Q.; Bando, Y.; Zhan, J. H.; Li, Y. B.; Sekiguchi, T. *Appl. Phys. Lett.* **2003**, *83*, 4414.
(43) Peulon, S.; Lincot, D. *J. Electrochem. Soc.* **1998**, *145*, 864.

Table 2. Comparison of the Crystallographic Orientation Index M(*hkl*), Lattice Parameters, and the Band Gap E_g for ZnO Nanowalls, Nanodisks, Nanospikes, and Nanopillars

	$M(hkl)^{a,b}$								lattice parameters (Å)		
ZnO	(100) (10$\bar{1}$0)	(002) (0001)	(101) (10$\bar{1}$1)	(102) (10$\bar{1}$2)	(110) (11$\bar{2}$0)	(103) (10$\bar{1}$3)	(112) (11$\bar{2}$2)	(201) (20$\bar{2}$1)	$a = b$	c	E_g (eV) ±0.1
nanowalls	1.213	1.150	0.795	0.970	1.212	0.894	0.957	1.028	3.2497	5.2096	3.27
nanodisks	0.786	1.278	0.860	1.117	1.232	1.058	1.185	0.971	3.2606	5.2325	3.25
nanospikes	0.819	1.496	0.798	1.264	0.797	1.376	1.085	0.914	3.2575	5.2206	3.12
nanopillars	0.267	3.541	0.298	0.985	0.454	2.218	0.557	0.285	3.2532	5.2053	3.15

[a] The crystallographic orientation index is given by $M(hkl) = [I(hkl)/\sum I(hkl)]/[I_0(hkl)/\sum I_0(hkl)]$, where $I(hkl)$ and $I_0(hkl)$ are the XRD peak areas from the experimental pattern and from the reference pattern (JCPDS 01-076-0704), respectively. [b] The corresponding plane notations for the XRD (*hkl*) assignments are indicated in the second row.[5]

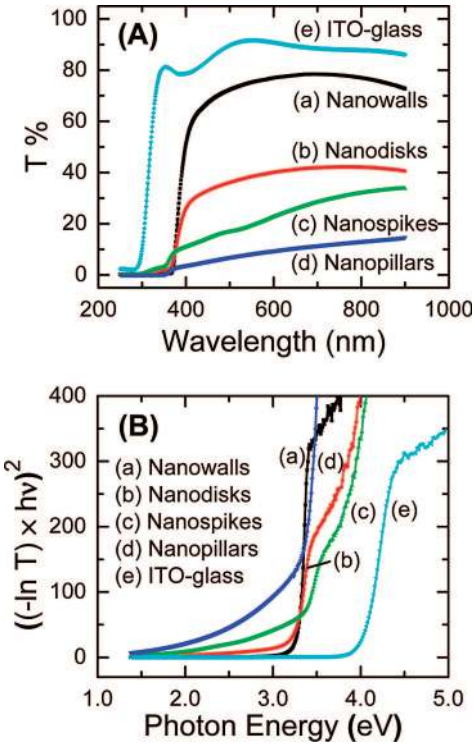

Figure 4. (A) Optical transmittance (T) spectra for (a) ZnO nanowalls, (b) nanodisks, (c) nanospikes, and (d) nanopillars electrodeposited on ITO-glass at 70 °C and for (e) bare ITO-glass. (B) The corresponding bandgaps are estimated from the zero-crossing values obtained by extrapolation of a linear fit to the rising edges of the respective $[(-\ln T)h\nu]^2$ vs photon energy plots.

nanostructures generally depends on several factors, including morphology, crystal density, surface roughness, and defects in the samples.[44] In the present case, the reduction in *T*% with different nanostructures could be attributed to the surface coverage of the respective ZnO nanostructures on the substrate. The voids between the vertically grown nanowalls (>500 nm, Figure 1b) are found to be considerably larger than those between the nanopillars (<200 nm, Figure 1h). Although the formation of byproducts (e.g., chlorinated salts) during electrodeposition[19] could also reduce the *T*% for nanospikes and nanopillars, this possibility can be ruled out for nanopillars in the present work by the absence of their signatures in our EDX (Figure 2b) and XRD spectra (Figure 3A, curve d). It should also be noted that the *T*% could be improved by postannealing of the as-deposited ZnO nanostructures.[27] Furthermore, the morphology can also play a major role on the transparency of the ZnO film. The recent study by Gao et al. showed that ZnO flake-type films have a higher transparency than rod-type films.[45] This is in good accord with the present study that shows a higher transparency for the 2D nanostructures relative to the 1D nanostructures.

Theoretical investigation using a combination of tight-binding and effective-potential methods shows changes in the band gap of ZnO nanowires when the diameter is smaller than 5 nm.[46] As the sizes of our nanostructures are greater than 50 nm, i.e., well above the quantum-size limit,[46] we have estimated their band gaps from the UV−vis data using the conventional Tauc equation[47,48]

$$\alpha h\nu = A(h\nu - E_g)^{n/2} \quad (1)$$

where $n = 1$ for a direct and $n = 4$ for an indirect band gap and A is an empirical constant. As ZnO is known to be a typical direct bandgap semiconductor,[49] the optical band gap (E_g) of these materials can be estimated from the zero-crossing value obtained by extrapolation of a linear fit to the rising edge of the $(\alpha h\nu)^2$ versus $h\nu$ plot (Figure 4B), where $h\nu$ is the photon energy and α (=−ln T) is the absorbance.[27,50] The corresponding estimated band gap values for the ZnO nanostructures are summarized in Table 2. The estimated optical band gaps of the nanospikes (3.12 eV) and nanopillars (3.15 eV) are found to be smaller than those of nanodisks (3.25 eV) and nanowalls (3.27 eV). The measured optical gaps of these electrochemically synthesized nanostructures are evidently all smaller than the theoretical value of ZnO (3.37 eV), but the observed overall range is well within the limit of ZnO thin films and nanopowders.[23,51] It should be noted that the bandgap values of nanowalls and nanodisks are also found to be close to that of the ZnO nanowires array film obtained by Gao et al. using a solution-based method with $ZnCl_2$ as the starting material at a higher deposition temperature of 95 °C.[52]

3.4. X-ray photoelectron spectroscopic study. The surface composition of the ZnO nanostructures as a function of sputtering time has been determined by XPS. The corresponding survey spectra (not shown) reveal primarily Zn and O features, along with negligible amounts of C and Cl. Although C is commonly found as a surface contaminant and can easily be removed after light sputtering (<300 s), the observed Cl features persist throughout the etch layers in the cases of nanowalls and nanodisks, but only in small quantity in nanospikes and not at all in nanopillars. This strongly suggests the important role of Cl^- ions in the formation of 2D ZnO nanostructures (see later).

(44) Yamamoto, T.; Shiosaki, T.; Kawabata, A. *J. Appl. Phys.* **1980**, *51*, 3113.
(45) Gao, Y. -F.; Miao, H. -Y.; Luo, H. -J.; Nagai, M.; Shyue, J. -J *J. Phys. Chem. C* **2008**, *112*, 1498.
(46) Pedersen, T. G. *Phys. Status Solidi C* **2005**, *2*, 4026.
(47) Tauc, J.; Menth, A. *J. Non-Cryst. Solids* **1972**, *8−10*, 569.
(48) Wang, Y. S.; Thomas, P. J.; O'Brien, P. *J. Phys. Chem. B* **2006**, *110*, 21412.
(49) Pankove, J. I. *Optical Processes in Semiconductors*; Prentice-Hall: Englewood Cliffs, NJ, 1979.
(50) Hong, R.; Shao, J.; He, H.; Fan, Z. *Appl. Surf. Sci.* **2006**, *252*, 2888.
(51) Dutta, S.; Chattopadhyay, S.; Jana, D.; Banerjee, A.; Manik, S.; Pradhan, S. K.; Sutradhar, M.; Sarkar, A. *J. Appl. Phys.* **2006**, *100*, 114328.
(52) Gao, Y.; Nagai, M.; Chang, T.-C.; Shyue, J.-J. *Cryst. Growth Des.* **2007**, *7*, 2467.

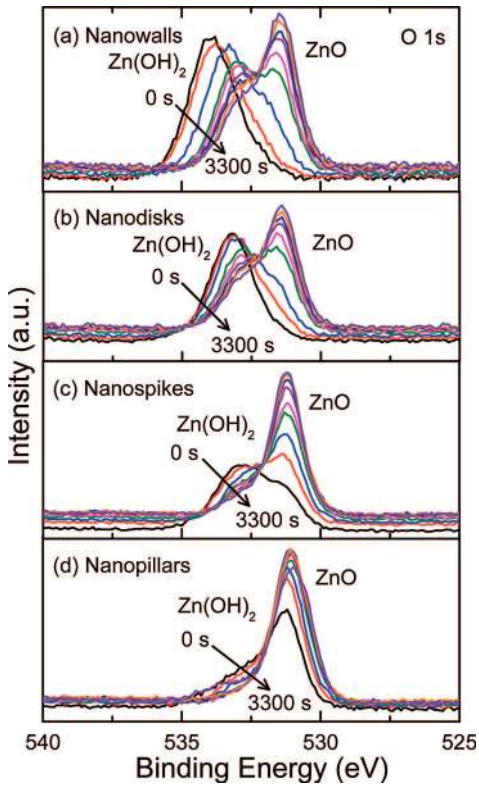

Figure 5. The O 1s XPS spectra of (a) nanowalls, (b) nanodisks, (c) nanospikes, and (d) nanopillars deposited on ITO-glass at 70 °C and upon ion sputtering for 0, 30, 60, 180, 240, 300, 900, 1500, and 3300 s.

Figure 5 shows the O 1s XPS spectra for the ZnO nanostructures as a function of sputtering time. Evidently, the O 1s envelope for the as-deposited ZnO nanowalls (Figure 5a) can be fitted to two components attributed to $Zn(OH)_2$ at 533.8 eV and ZnO at 532.2 eV. Upon sputtering for 3300 s, the entire envelope is found to gradually shift to a lower BE, with the $Zn(OH)_2$ and ZnO components settling at 532.9 and 531.4 eV, respectively. These O 1s features are located 0.5−1.0 eV higher in BE than the most reported values,[53,54] which can be attributed to differential sample charging caused by the presence of a residual amount of the nonconducting $Zn(OH)_2$. However, the BE difference of the two O 1s components remains the same at 1.5 ± 0.1 eV throughout sputtering, which is in good accord with the reported BE difference of 1.5 eV[55] to 2.0 eV.[56] The presence of $Zn(OH)_2$ is not surprising because $Zn(OH)_2$ is an intermediate in the electrochemical reaction for the formation of ZnO[19] and hydroxyl compounds are known to form in electrodeposition with a Zn^{2+} concentration above 0.01 M.[43] A certain amount of $Zn(OH)_2$ could remain without being completely converted to ZnO. Furthermore, electrochemical synthesis of ZnO in an aqueous solution and the subsequent washing in Millipore water also naturally produce $Zn(OH)_2$ at the surface of the working electrode. A similar kind of XPS spectrum has also been obtained for ZnO thin films synthesized by ion gas layer reaction.[54] In addition, sputtering also reduces the $Zn(OH)_2$ component while concomitantly increasing the ZnO component, which suggests that the bulk of the nanostructure is predominantly ZnO and is

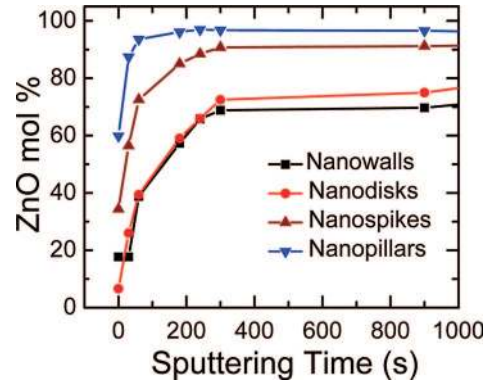

Figure 6. The ZnO mol % as a function of sputtering time for ZnO nanostructures deposited on ITO-glass at 70 °C.

covered by a $Zn(OH)_2$ outer layer. For nanodisks (Figure 5b), we also observe similar spectral evolution upon sputtering, indicating that the nanodisks have a similar composition makeup as the nanowalls. However, in the case of 1D ZnO nanostructures, i.e., nanospikes (Figure 5c) and nanopillars (Figure 5d), the $Zn(OH)_2$ to ZnO O 1s intensity ratio is significantly less than that of the 2D nanostructures (Figure 5a,b). This can be explained on the basis of the lower electrolyte concentrations (0.01 and 0.001 M $Zn(NO_3)_2 \cdot 6H_2O$) used to grow these 1D nanostructures, where the slower hydroxylation reaction kinetics allows formation of lesser $Zn(OH)_2$.

The mol % of ZnO in these nanostructures can be estimated by the ratio of the area under the ZnO O 1s fitted curve to the sum of the ZnO O 1s fitted area and one-half of the $Zn(OH)_2$ O 1s fitted area. The relative changes of this ZnO mol % as a function of sputtering time for different nanostructures are shown in Figure 6. After sputtering for 300 s, the ZnO mol % for all the nanostructures becomes essentially constant. In particular, the ZnO mol % values after 900 s sputtering for nanowalls (70 mol %) and nanodisks (75 mol %) are substantially less than the corresponding values for nanospikes (91 mol %) and nanopillars (97 mol %). Indeed, the ZnO mol % value follows the same ordering (nanowalls < nanodisks < nanospikes < nanopillars) at any given total sputtering time. This also parallels the opposite trend as the electrolyte concentration used to grow the respective nanostructures (nanowalls (0.1 M) > nanodisks (0.05 M) > nanospikes (0.01 M) > nanopillars (0.001 M)), which suggests that the dehydration reaction ($Zn(OH)_2(s) \rightarrow ZnO(s) + H_2O(l)$) is slower than the hydroxylation reaction ($Zn^{2+}(aq) + 2OH^-(aq) \rightarrow Zn(OH)_2(s)$) at a higher electrolyte concentration—see later. In the case of nanopillars with 97 mol % ZnO, part of the residual amount of $Zn(OH)_2$ could also be due to rapid surface hydroxylation under vacuum as proposed by Purchert et al., who observed the presence of both ZnO and $Zn(OH)_2$ in situ by XPS even on a ZnO single crystal surface freshly cleaved under vacuum.[53]

Figure 7 compares the corresponding Zn 2p XPS spectra of different ZnO nanostructures. The intense Zn $2p_{3/2}$ ($2p_{1/2}$) feature indicates the presence of a single Zn^{2+} divalent state, corresponding to both $Zn(OH)_2$ and ZnO. The spin−orbit splitting of 23.0 ± 0.1 eV is evidently in good accord with the literature value of 22.97 eV.[57] The shifting of the Zn 2p features to a lower BE position upon sputtering parallels the spectral evolution of the O 1s features (Figure 5), which could again be attributed to differential charging effect due to the presence of nonconducting

(53) Puchert, M. K.; Timbrell, P. Y.; Lamb, R. N. *J. Vac. Sci. Technol., A* **1996**, *14*, 2220.
(54) Bär, M.; Reichardt, J.; Sieber, I.; Grimm, A.; Kötschau, I.; Lauermann, I.; Sokoll, S.; Lux-Steiner, M. C.; Fischer, C. H.; Niesen, T. P. *J. Appl. Phys.* **2006**, *100*, 23710.
(55) Deroubaix, G.; Marcus, P. *Surf. Interface Anal.* **1992**, *18*, 39.
(56) Au, C. T.; Roberts, M. W.; Zhu, A. R. *Surf. Sci.* **1982**, *115*, L117.
(57) Moulder, J. F.; Stickle, W. F.; Sobol, P. E.; Bomben, K. D. *Handbook of X-ray Photoelectron Spectroscopy*; Chastain, J., Ed.; Perkin-Elmer Corp.: Eden Prairie, MN, 1992.

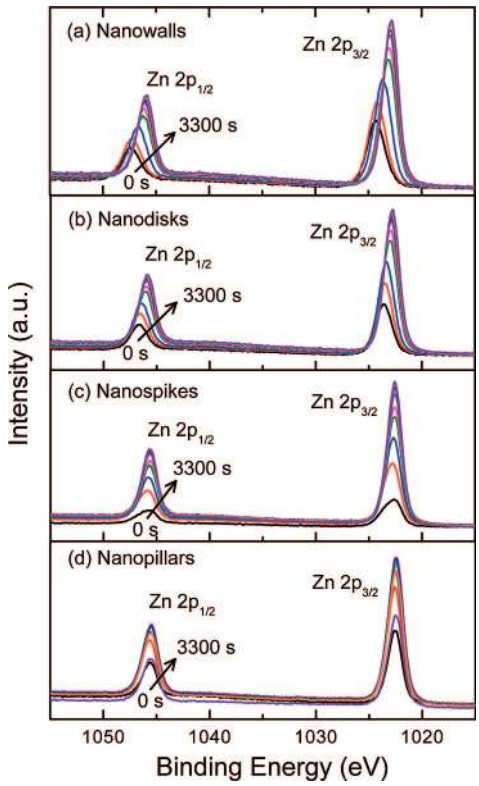

Figure 7. The Zn 2p XPS spectra of (a) nanowalls, (b) nanodisks, (c) nanospikes, and (d) nanopillars as deposited on ITO-glass at 70 °C and upon ion sputtering for 0, 30, 60, 180, 240, 300, 900, 1500, and 3300 s.

$Zn(OH)_2$. Furthermore, the increase in the overall Zn 2p intensity with increasing sputtering time is consistent with the higher Zn density in the ZnO core than that of the $Zn(OH)_2$ outer layer. Upon sputtering for 3300 s, the Zn $2p_{3/2}$ ($2p_{1/2}$) feature appears to settle at 1022.8 eV (1045.9 eV) for nanowalls, 1022.8 eV (1045.9 eV) for nanodisks, 1022.5 eV (1045.6 eV) for nanospikes, and 1022.4 eV (1045.5 eV) for nanopillars. The resulting BE position of Zn 2p in nanopillars is lowest likely due to the high mole percentage (>95%) of ZnO (Figure 6).

In addition to the prominent Zn 2p and O 1s features, we also observe prominent Cl features in the case of 2D nanostructures (nanowalls and nanodisks) and weaker Cl features in the nanospikes but not in the nanopillars, which is consistent with our corresponding EDX data (Table 1). Parts a and b of Figure 8 show the Cl 2p XPS spectra of ZnO nanowalls and nanopillars, respectively, as deposited at 70 °C and as a function of sputtering time. The Cl 2p spectral evolution with sputtering for nanodisks is found to be similar to that of nanowalls. The Cl 2p envelope consists of Cl $2p_{3/2}$ and Cl $2p_{1/2}$ features with a spin−orbit splitting of 1.6 eV. The total intensity of the Cl 2p envelope appears to become constant after 60 s of sputtering (Figure 8), and the apparent lower Cl intensity observed in the top layers could be due to rinsing of samples in Millipore water after the deposition. Furthermore, because the hydroxyl compounds ($Zn_5(OH)_8Cl_2 \cdot H_2O$) contain both OH and Cl groups and the $Zn(OH)_2$ mol % is found to decrease with increasing sputtering time (as shown in Figures 5 and 6), the initial increase in the Cl 2p intensity with sputtering time cannot be entirely attributed to the hydroxyl compounds. Moreover, the significant presence of Cl throughout the 2D nanostructures therefore suggests its important role in the formation mechanism. The presence of a smaller quantity of Cl is believed to favor lateral growth in nanospikes, resulting in larger diameters (200−500 nm), as similarly found in the nanowire

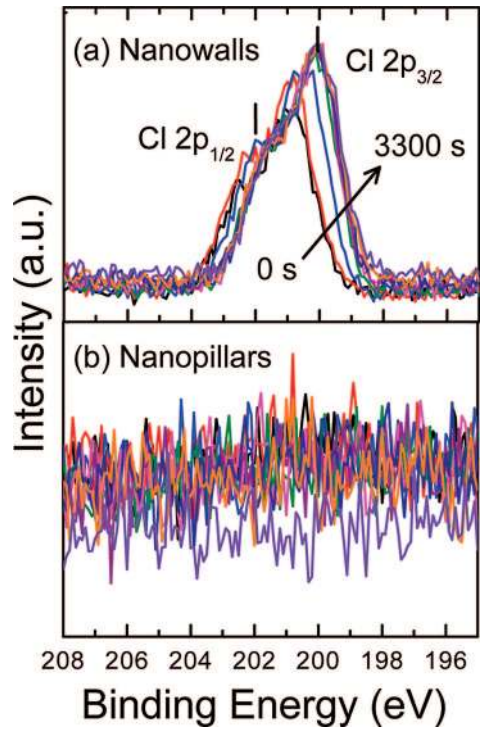

Figure 8. The Cl 2p XPS spectra of (a) ZnO nanowalls and (b) nanopillars as deposited on ITO-glass at 70 °C and upon ion sputtering for 0, 30, 60, 180, 240, 300, 900, 1500, and 3300 s.

study reported by Tena-Zaera et al.[29] The absence of Cl features in the nanopillars (Figure 8b), which grow in the [0001] direction, further supports the role of Cl in the capping of (0001) plane in the formation of the 2D nanostructures.

3.5. Growth Mechanism. In the electrochemical deposition of ZnO from $Zn(NO_3)_2$ electrolyte, the Zn^{2+} ions react with the OH^- ions to form $Zn(OH)_2$ (hydroxylation) prior to the conversion to ZnO (dehydration) according to the following well-known mechanism:[18]

$$Zn(NO_3)_2(aq) \rightleftharpoons Zn^{2+}(aq) + 2NO_3^-(aq) \quad (2)$$

$$NO_3^-(aq) + H_2O(l) + 2e^- \rightleftharpoons NO_2^-(aq) + 2OH^-(aq) \quad (3)$$

$$Zn^{2+}(aq) + 2OH^-(aq) \xrightarrow{k_{hydroxy}} Zn(OH)_2(s) \quad (4)$$

$$Zn(OH)_2(s) \xrightarrow{k_{dehyd}} ZnO(s) + H_2O(l) \quad (5)$$

The Zn^{2+} and NO_3^- ions are formed in the dissolution reaction of the zinc nitrate salt (eq 2), and the resulting NO_3^- ions are subsequently reduced to NO_2^- ions forming OH^- ions (eq 3). The electrochemical reduction of nitrate is often used in the electrodeposition of metal oxides[58–60] and hydroxides.[61,62] As the reaction mechanism involves the hydroxylation reaction (i.e., formation of $Zn(OH)_2$), the higher moieties of $Zn(OH)_2$ observed in the nanowalls and nanodisks are due to the use of higher $Zn(NO_3)_2$ electrolyte concentrations (0.1 and 0.05 M, respectively), at which hydroxylation occurs at a much faster rate on

(58) Natarajan, C.; Nogami, G. *J. Electrochem. Soc.* **1996**, *143*, 1547.
(59) Zhitomirsky, I.; Gal-Or, L.; Kohn, A.; Hennicke, H. W. *J. Mater. Sci.* **1995**, *30*, 5307.
(60) Zhou, Y.; Phillips, R. J.; Switzer, J. A. *J. Am. Ceram. Soc.* **1995**, *78*, 981.
(61) Matsumoto, Y.; Adachi, H.; Hombo, J. *J. Am. Ceram. Soc.* **1993**, *76*, 769.
(62) Streinz, C.; Hartman, A. P.; Motupally, S.; Weidner, J. W. *J. Electrochem. Soc.* **1995**, *142*, 1084.

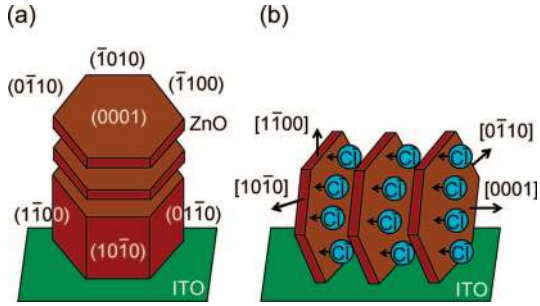

Figure 9. Schematic diagrams of (a) 1D and (b) 2D growth of ZnO nanostructures on ITO-glass. Nanospikes and nanopillars grow on the preferred plane (0001) forming the 1D nanostructures (a). In the case of nanowalls and nanodisks, Cl^- ions cap the (0001) facet of ZnO and thereby redirect growth on the $(10\bar{1}0)$ plane, forming the 2D nanostructures (b).

the electrode surface before complete dehydration to ZnO (i.e., $k_{hydroxy} > k_{dehyd}$). At a lower electrolyte concentration of 0.01 and 0.001 M, the $Zn(OH)_2$ component is reduced as demonstrated in the case of nanospikes and nanopillars, respectively, because $Zn(OH)_2$ is converted to ZnO as soon as it is produced (i.e., $k_{hydroxy} \leq k_{dehyd}$).

ZnO has been found to grow naturally along the $\pm$[0001] direction,[13,27,63] producing the 1D nanostructures (nanospikes and nanopillars) in the case of low $Zn(NO_3)_2$ electrolyte concentration (0.01 M, 0.001 M), as shown schematically in Figure 9a. At a higher electrolyte concentration (0.1 M, 0.05 M), the resulting fast hydroxylation kinetics overcomes the preferred growth direction in [0001], allowing growth in other directions. In the present work, we observe 2D nanostructures (nanowalls and nanodisks) at high electrolyte concentration but only in the presence of the supporting KCl electrolyte (used to enhance the conductivity of the solution). As shown in Figures 2a and 8 the presence of Cl in substantial quantity is detected in our EDX and XPS spectra, respectively, in the case of 2D nanostructures, despite the use of 0.1 M KCl supporting electrolyte for all the depositions. Although the ZnO crystal growth rate is five times faster on the (0001) planes than that on the $(10\bar{1}0)$ and $(01\bar{1}0)$ planes,[25] the adsorption of the highly electronegative Cl^- ions on the polar $\pm$(0001) plane is believed to hinder the growth in this direction, redirecting the growth on the (nonpolar) $(10\bar{1}0)$ plane.[37] The resulting nanostructures therefore have the preferred growth direction of $[10\bar{1}0]$ and appear 2D, as illustrated in Figure 10b. Yoshida et al. also reported the formation of circular stacking ZnO disks and suggested the adsorption of tetrasulfonated metallophthalocyanines onto the (0001) plane of ZnO as the mechanism for redirected growth on the $(10\bar{1}0)$ plane.[35] It should be noted that while we expect that similar adsorption of Cl^- ions would have occurred on the polar $\pm$(0001) plane in the case of low $Zn(NO_3)_2$ electrolyte concentration, the slow hydroxylation kinetics allows sufficient time for ion exchange, hence preventing significant surface capping by Cl^- ions (in contrast to that observed in the high concentration case). However, at a sufficiently high concentration of KCl (>0.1 M), the capping effect of Cl will occur. Recently, Tena-Zaera et al. observed enhanced growth in the lateral direction in ZnO nanowires, resulting in an increase in diameter from 80 to 300 nm, upon increasing the KCl concentration above 1 M.[29]

To verify the important role of the Cl^- ions in the generation of these 2D nanostructures, we repeat our deposition experiment using the same conditions for producing ZnO nanowalls but without the supporting KCl electrolyte. The SEM images shown

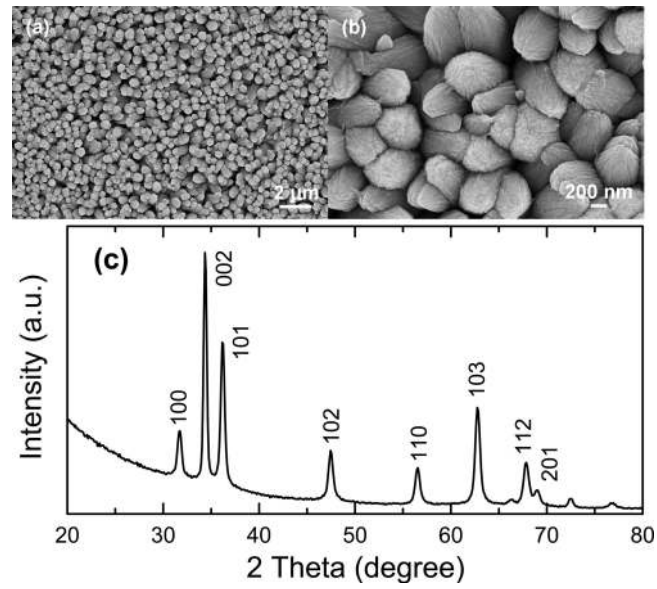

Figure 10. (a, b) SEM images of ZnO nanostructures grown on ITO-glass at 70 °C with 0.1 M $Zn(NO_3)_2 \cdot 6H_2O$ without any supporting KCl electrolyte and (c) GIXRD pattern of the corresponding ZnO nanostructures.

in panels a and b of Figure 10 reveal large pillar-like nanostructures with very rough surfaces, confirming the lack of 2D symmetry and of the preferred growth directions in the $(10\bar{1}0)$ plane. The corresponding GIXRD spectrum (Figure 10c) also supports the preferential growth in the [0001] direction, indicating a generally 1D nanostructure in accord with the SEM images. It is important to note that no additional XRD features other than those for the wurtzite ZnO structure are observed from these large pillar-like structures, which is consistent with the absence of $Zn_5(OH)_8Cl_2 \cdot H_2O$ even at a higher electrolyte concentration (0.1 M). This result illustrates that the presence of a capping agent is essential for producing 2D ZnO nanostructures by electrodeposition.

4. Conclusions

In the present work, we demonstrate that electrochemical deposition is a powerful method to synthesize ZnO nanostructures of both 2D (nanowalls and nanodisks) and 1D (nanospikes and nanopillars) on ITO-glass substrates. X-ray diffraction studies confirm that these nanomaterials are highly crystalline wurtzite structure, similar to that observed in the vapor-phase growth of ZnO.[14] Optical direct band gaps of these ZnO nanostructures are found to be 3.12−3.27 eV from UV−vis spectroscopy. The concentration of the $Zn(NO_3)_2 \cdot 6H_2O$ electrolyte solution (at carefully controlled deposition temperature) plays a crucial role in building these novel self-assembled nanostructured materials. Depth-profiling XPS studies reveal that the nanostructures consist of a ZnO core covered by a $Zn(OH)_2$ outer layer. The larger $Zn(OH)_2$ moiety found for the 2D relative to the 1D nanostructures is due to the faster hydroxylation kinetics, as a result of the higher $Zn(NO_3)_2$ electrolyte concentration used for the 2D nanostructure deposition. In addition, the presence of substantial Cl is detected in the 2D nanostructures (nanowalls and nanodisks), indicating its important role in hindering growth in the (0001) plane. Following the earlier suggestion,[35,37] we propose a growth model for 2D nanostructures (Figure 9) that involves capping of the polar (0001) plane by Cl^- ions in the fast hydroxylation kinetics conditions. Furthermore, this mechanism has been

(63) Choi, Y.-J.; Park, J. -H.; Park, J. -G *J. Mater. Res.* **2005**, *20*, 959.

independently verified with the formation of only 1D nanostructures (wide nanopillars) when the KCl supporting electrolyte is removed. The present electrochemical method therefore offers morphological control in the formation of diverse ZnO nanostructures on ITO-glass at relatively low temperature and catalyst-free conditions. These ZnO nanostructures promise further opportunities for green energy (solar cells), field emission, and sensor applications.

Acknowledgment. This work was supported by the Natural Sciences and Engineering Research Council of Canada.

LA8008943